Astronomy & Astrophysics manuscript no. 44652girardi
January 28, 2023

A newly identified galaxy group thanks to tidal streams of intragroup light ⋆

M. Girardi[1,2], S. Zarattini[3,4], W. Boschin[5,2,6,7], M. Nonino[2], I. Bartalucci[8], A. Mercurio[9,10], N. Nocerino[1], P. Rosati[11]

[1] Dipartimento di Fisica dell'Università degli Studi di Trieste - Sezione di Astronomia, via Tiepolo 11, I-34143 Trieste, Italy e-mail: marisa.girardi@inaf.it
[2] INAF - Osservatorio Astronomico di Trieste, via Tiepolo 11, I-34143 Trieste, Italy
[3] Dipartimento di Fisica e Astronomia "G. Galilei", Università di Padova, vicolo dell'Osservatorio 3, I-35122 Padova, Italy
[4] INAF - Osservatorio Astronomico di Padova, vicolo dell'Osservatorio 2, I-35122 Padova, Italy
[5] Fundación Galileo Galilei - INAF (Telescopio Nazionale Galileo), Rambla José Ana Fernández Perez 7, E-38712 Breña Baja (La Palma), Canary Islands, Spain
[6] Instituto de Astrofísica de Canarias, C/Vía Láctea s/n, E-38205 La Laguna (Tenerife), Canary Islands, Spain
[7] Departamento de Astrofísica, Univ. de La Laguna, Av. del Astrofísico Francisco Sánchez s/n, E-38205 La Laguna (Tenerife), Spain
[8] INAF - Istituto di Astrofisica Spaziale e Fisica Cosmica di Milano, Via A. Corti 12, I-20133 Milano, Italy
[9] Dipartimento di Fisica E.R. Caianiello, Università Degli Studi di Salerno, Via Giovanni Paolo II, I-84084 Fisciano (SA), Italy
[10] INAF - Osservatorio Astronomico di Capodimonte, via Moiariello 16, I-80131 Napoli, Italy
[11] Dipartimento di Fisica e Scienze della Terra, Università di Ferrara, via Saragat 1, I-44122 Ferrara, Italy

Received / Accepted

ABSTRACT

Context. In the accretion-driven growth scenario, part of the intracluster light is formed in the group environment.
Aims. We report the serendipitous discovery of a group of galaxies with signs of diffuse light in the foreground of the known galaxy cluster MACS J0329-0211 at $z \sim 0.45$.
Methods. Our investigation began with the detection of diffuse light streams around a pair of bright galaxies in the southeastern region of a Suprime-Cam image of the galaxy cluster MACS J0329-0211. Our analysis is based on the extended CLASH-VLT redshift catalog and on new spectroscopic data obtained ad hoc with the Italian Telescopio Nazionale *Galileo*. We use the density reconstruction method to analyze the redshift distribution of the galaxies in the region around the galaxy pair. We also use available photometric and X-ray data to better characterize the properties of the group.
Results. Thanks to the large amount of redshift data collected in this region, we have been able to discover the existence of a group of galaxies, here called GrG J0330-0218, which is associated with the pair of galaxies. These are the two brightest group galaxies (BGG1 and BGG2). We extracted 41 group members from the redshift catalog and estimate a mean redshift $z = 0.1537$ and a line-of-sight velocity dispersion $\sigma_V \sim 370$ km s^{-1}. In the phase-space diagram, the distribution of the galaxies of GrG J0330-0218 follows the characteristic trumpet-shaped pattern, which is related to the escape velocity of galaxy clusters, suggesting that the group is a virialized structure. Under this assumption, the mass of the group is $M_{200} \sim 6 \times 10^{13}\ M_\odot$. We also measured a mass-to-light ratio of $\sim 130\ M_\odot/L_\odot$ and a luminosity fraction of diffuse light of $\sim 20\%$ within $0.5\ R_{200}$.
Conclusions. We conjecture that galaxy pairs that are surrounded by diffuse light, probably due to tidal interactions, can serve as signposts for groups.

Key words. Galaxies: groups: individual: GrG J0330-0218 – Galaxies: groups: general – Galaxies: clusters: individual: MACS J0329-0211 – Galaxies: clusters: general – Galaxies: kinematics and dynamics

1. Introduction

Galaxy clusters evolve and increase in mass through a hierarchical merging process from poor groups to rich clusters. As shown by numerical simulations, accretion of smaller systems at the galaxy or group scale is the main channel of cluster growth (e.g., Benavides et al. 2020 and references therein). In this scenario, some of the intracluster diffuse light could originate from the group environment.

Diffuse light is the light from stars that float freely in the gravitational potential of galaxy systems and that are not bound to a galaxy. For simplicity, we use the term ICL when referring to both intragroup and intracluster light. Diffuse light in galaxy systems was first discovered by Zwicky (1951) in the Coma cluster and studied in the following years. We refer to Contini (2021) and Montes (2022) as two very recent reviews on this topic. Most of the ICL in clusters is concentrated around the brightest cluster galaxy (BCG) where it is considered to be an extended component over the Sérsic light profile of the BCG itself.

To detect ICL there are three methods used in the literature. The most commonly used method for calculating the ICL is that based on a surface brightness cut (e.g., Feldmeier et al. 2004; Burke et al. 2012; Furnell et al. 2021). It assumes that all light below a certain surface brightness can be fully attributed to the ICL. The disadvantage of this method is that images with dif-

⋆ Full Table 1 is only available in electronic form at the CDS via anonymous ftp to cdsarc.cds.unistra.fr (130.79.128.5) or via https://cdsarc.cds.unistra.fr/cgi-bin/qcat?J/A+A/

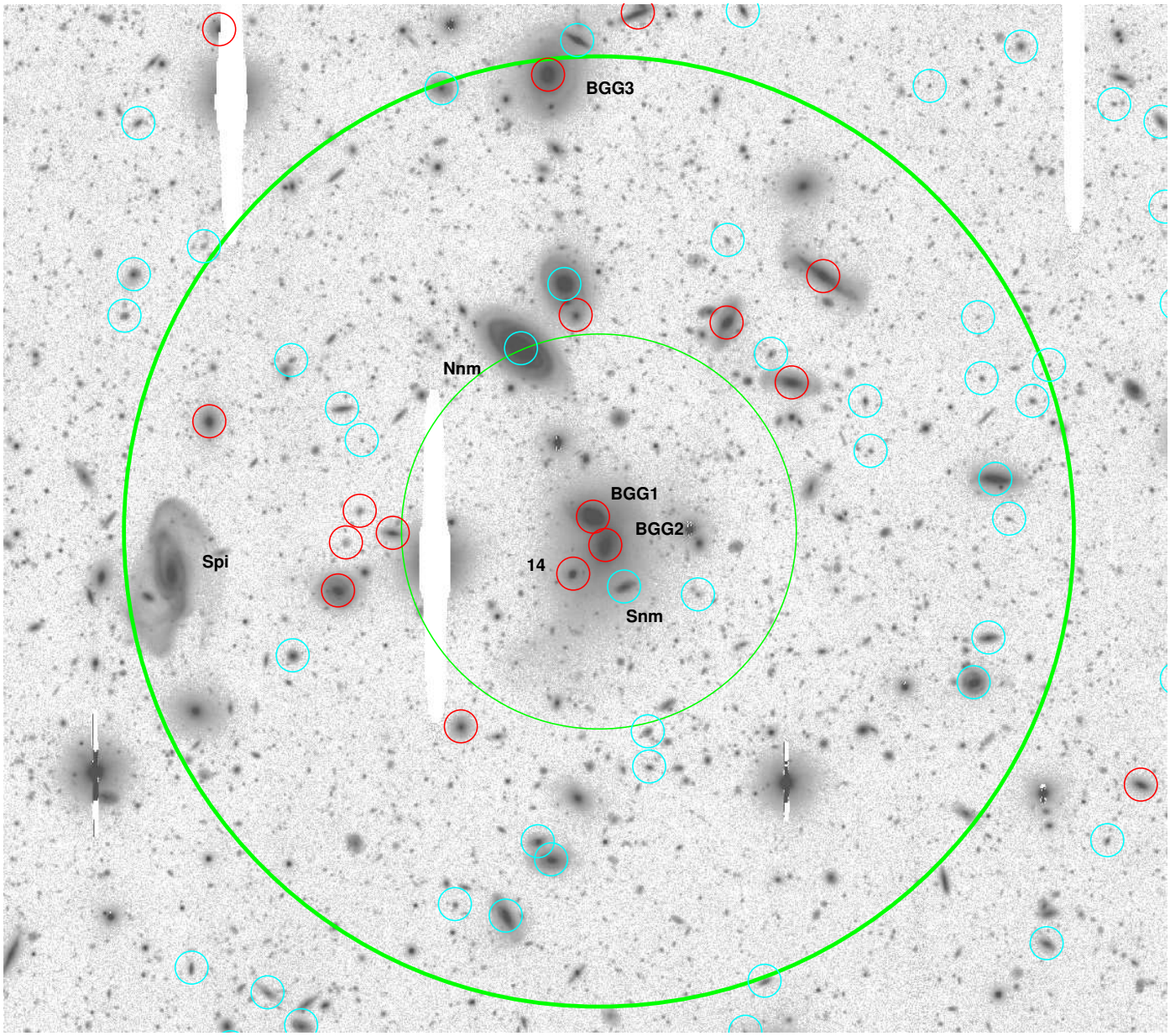

Fig. 1. Southeastern region of the Suprime-Cam R_C-band image of the cluster MACS0329 (north top and east left) showing the group region within 0.5 R_{200} ∼ 2.4′ (enclosed in the large, thick green circle). The thin green circle indicates the 1′ radius region (1′ ∼ 160 kpc at the group redshift). Galaxies with available redshift are highlighted with small circles, in particular red or cyan circles in the case of members or nonmembers according to the selection procedure (see Sects. 2 and 3). Labels indicate objects discussed in the text.

ferent exposure times for the same galaxy cluster give different amounts of the ICL (e.g., Montes & Trujillo 2018). Moreover, it does not account for the ICL that overlaps with the BCG in the transition region. As an alternative method, BCG and ICL light can be described by adding separate models for the two components. This method based on the surface brightness profile fit can be heavily degenerate (e.g., Janowiecki et al. 2010). Moreover, as pointed out by Montes & Trujillo (2018), it also fails to account for ICL not concentrated around the BCG, asymmetries in the light distribution, and substructures such as tidal streams. The third approach is based on 2D techniques, such as fitting algorithms to take into account most of the galaxies in the cluster (e.g., Giallongo et al. 2014; Presotto et al. 2014; Cattapan et al. 2019) or wavelet-like decomposition techniques (e.g., Ellien et al. 2021).

Indeed, it is not easy to understand whether the observed diffuse light is bound to the BCG or to the cluster (true ICL), if one uses only imaging (e.g., Kluge et al. 2021; Montes et al. 2021). As numerical simulations suggest (e.g., Dolag et al. 2010), the population of ICL stars should have a higher velocity dispersion than BCG stars and be more similar to that of the host cluster. This can be observed in a few cases where detailed spectroscopic studies can be performed, such as when studying the kinematics of planetary nebulae or globular clusters around nearby BCGs (e.g., Arnaboldi et al. 1996; Longobardi et al. 2018; Alamo-Martínez et al. 2021). However, these tracers can only be used for very low redshift objects ($z << 0.1$). To our knowledge, there is only one cluster in which ICL occurs at the cluster center without the presence of a BCG, namely Abell 545 (Struble 1988; Barrena et al. 2011 and references therein). This case is clear ev-

idence that diffuse light is bound to the gravitational potential of the cluster.

Among the mechanisms for ICL formation in galaxy clusters, the most important are mass loss during galaxy mergers, tidal disruption of dwarf galaxies, tidal stripping of intermediate and massive galaxies, and accretion of ICL from groups also called preprocessing (see e.g., Contini 2021). Numerical simulations suggest that half of the ICL comes from galaxies associated with the family merger tree of BCGs in clusters (e.g., Murante et al. 2007) and that stellar stripping by an established cluster potential is stronger in the innermost region of the haloes and in clusters than in groups (Contini et al. 2018). On the other hand the mechanisms related to galaxy mergers and galaxy-galaxy encounters are favored in the group environment where the encounter velocity is low and comparable to the internal velocity of stars in galaxies. In fact, numerical simulations show as slow interactions between galaxies in the group environment lead to strong tidal stripping and the formation of tidal tails and streams that decay with time and evolve into a more diffuse and amorphous ICL envelope in the cluster environment (Rudick et al. 2006; Rudick et al. 2009).

According to Rudick et al. (2009), 40% of the cluster ICL is generated in streams and Contini et al. (2014) calculated that preprocessing can contribute up to 30% of the total ICL in massive clusters. The complex substructure of diffuse light in the Virgo cluster also suggests that ICL is related to the hierarchical nature of cluster assembly and is not the product of uniform accretion around a central galaxy (Mihos et al. 2005). The analysis of *James Webb* Space Telescope (JWST) data allows the detection of a lot of substructures in the ICL of distant clusters suggesting that one can observe the formation of the diffuse extended component in clusters (Montes & Trujillo 2022). Despite the presumed importance of the preprocessing mechanism for ICL formation in clusters, there is little evidence for ICL in groups. Mihos (2016) describes several cases of loose groups that show little evidence for ICL despite refined studies. ICL detection has been reported in a few cases (e.g., Castro-Rodríguez et al. 2003; Spavone et al. 2018; Cattapan et al. 2019, Raj et al. 2020). On the other hand, ICL detection is quite common in compact groups such as Stephan's quintet (Mendes de Oliveira et al. 2001), Seyfert's sextet (Durbala et al. 2008), and several other cases (e.g., Da Rocha & Mendes de Oliveira 2005; Cortese et al. 2006; Da Rocha et al. 2008; Poliakov et al. 2021; Ragusa et al. 2021), though not in all compact groups (e.g., Aguerri et al. 2006).

While inspecting an image taken with the Subaru Prime Focus Camera (Suprime-Cam) and centered on the galaxy cluster MACS J0329-0211 at $z \sim 0.45$ (hereafter MACS0329), we detected two bright galaxies in the southeastern region, likely in the foreground of MACS0329 and surrounded by strong diffuse light. In addition to the large amount of spectroscopic data in the region of MACS0329 obtained in the CLASH-VLT project, we performed new optical observations to obtain new spectroscopic data with the Italian Telescopio Nazionale *Galileo* (TNG) in the region around the two galaxies. Here we report the discovery of a group of galaxies, hereafter called GrG J0330-0218, associated with this pair of bright galaxies.

The paper is structured as follows. We describe the new observations and all optical data in Sect. 2. We present the selection of group members and the redshift catalog in Sect. 3. In Sects. 4 and 5 we present our results on the group structure, the two dominant galaxies, and the ICL. We give a brief overview of the study of the large-scale environment of GrG J0330-0218 in Sect. 6. Section 7 is devoted to the interpretation and discussion of our results. In Sect. 8, we give a brief summary and derive our conclusions. In this work we use $H_0 = 70$ km s^{-1} Mpc^{-1} in a flat cosmology with $\Omega_0 = 0.3$ and $\Omega_\Lambda = 0.7$. In the assumed cosmology, $1'$ corresponds to $\sim$ 160 kpc at the group redshift. Recall that the velocities we derive for the galaxies are line-of-sight velocities determined from the redshift, $V = cz$. Unless otherwise stated, we report errors with a confidence level (c.l.) of 68%.

2. Observations and data

Figure 1 shows the southeastern region of the Suprime-Cam image centered on MACS0329 where we detected two bright galaxies surrounded by diffuse light. These two galaxies are listed by NED[1] as the galaxy pair APMUKS(BJ) B032735.21-02283 (Maddox et al. 1990). Since these two galaxies will prove to be the two brightest galaxies of a group in the foreground of MACS0329, we refer to them as BGGs (BGG1 to the north and BGG2 to the south).

2.1. New spectroscopic TNG data

Long-slit spectroscopic observations of galaxies in the field of GrG J0330-0218 were performed in November and December 2015 and in January 2016 at the TNG. As instrument, we used the Device Optimized for LOw REsolution Spectroscopy (DOLoRes) with the LR-B grism. With LR-B Grm1 all the relevant spectral features can be observed at the group redshift , while the resolution is enough for the measurement of accurate galaxy redshifts. In total, we acquired spectra for 18 galaxies with exposure times between 900 s and 1800 s. These observations focused on the two galaxies BGG1 and BGG2 and on bright galaxies in their vicinity. The spectra of the two BGGs are shown in Fig. 2.

Spectral reduction and radial velocity estimation were performed using the standard IRAF[2] tasks and the cross-correlation technique (Tonry & Davis 1979). In our experience with DOLoRes in spectroscopic mode, the nominal velocity errors provided by the cross-correlation technique must be multiplied by a factor of 2–2.5 (e.g., Girardi et al. 2022). In this case, comparison of multiple velocity measurements for four galaxies suggests that we should be more conservative and allow for errors equal to the nominal errors multiplied by a factor of 3. In total, we obtained velocity estimates for 18 galaxies. The median value of the uncertainties in the velocity measurements is 112 km s^{-1}.

2.2. CLASH-VLT spectroscopic data

The galaxy cluster MACS0329 is part of the "Cluster Lensing And Supernova survey with Hubble" project (CLASH, Postman et al. 2012) and was surveyed with VIMOS as part of ESO Large Program 186.A-0798 "Dark Matter Mass Distributions of Hubble Treasury Clusters and the Foundations of LCDM Structure Formation Models" (PI: P. Rosati). This program is the panoramic spectroscopic survey of the 13 CLASH clusters visible from ESO-Paranal, named CLASH-VLT (Rosati et al. 2014; Rosati et al. in prep.). VIMOS was used with both the low-resolution blue grism (LRb) and the medium-resolution grism (MR) with typical cz errors of 150 and 75 km s^{-1}, respectively

[1] http://ned.ipac.caltech.edu/

[2] IRAF is distributed by the National Optical Astronomy Observatories, which are operated by the Association of Universities for Research in Astronomy, Inc., under a cooperative agreement with the National Science Foundation.

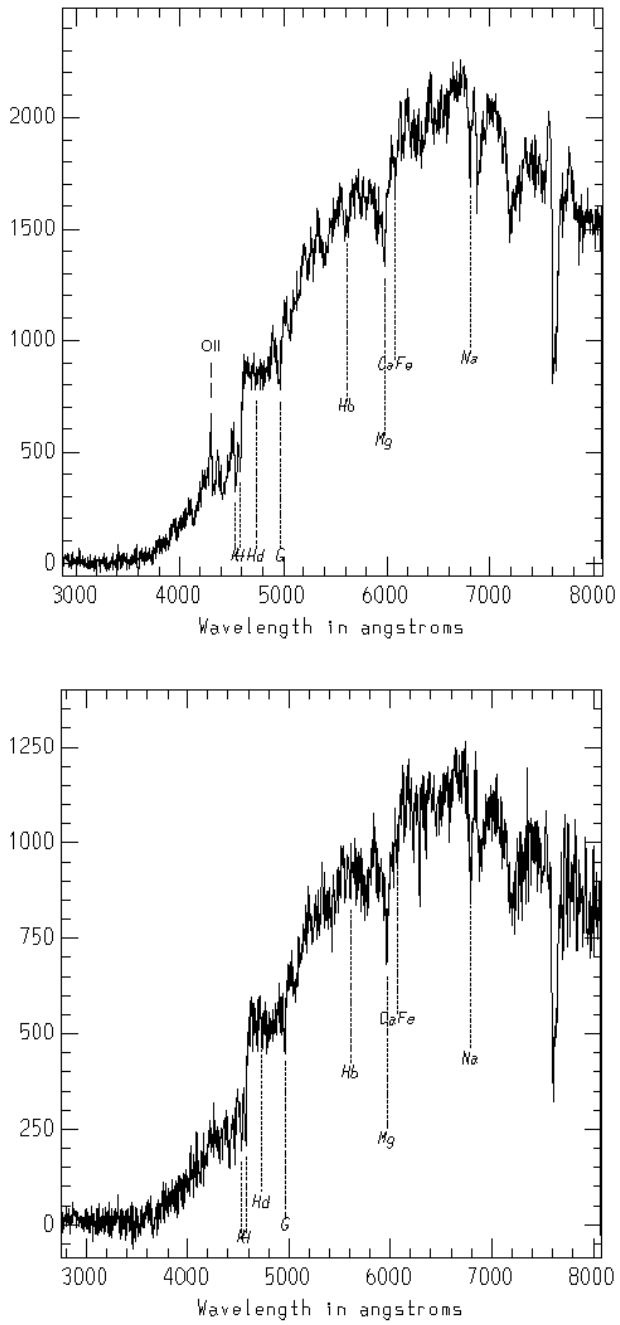

Fig. 2. TNG spectra of BGG1 and BGG2 in the upper and lower panels, respectively. ADU in y-axis.

(Balestra et al. 2016). Each redshift was also assigned a quality flag. Exact details of the CLASH-VLT data reduction can be found in the study by Mercurio et al. (2021). The wide-field VLT-VIMOS spectroscopy was complemented by VLT-MUSE spectroscopy with integral field in the central cluster regions (Caminha et al. 2019) with typical cz errors of 40 km s^{-1} (Inami et al. 2017).

For the MACS0329 field, we consider the 1712 galaxies of the CLASH-VLT catalog with redshift between 0 and 1. Of these, 1637 galaxies are from VIMOS, 74 from MUSE, and one additional bright galaxy is from a TNG long-slit observation. In particular, we only considered VIMOS redshifts with a quality flag QF$\geq$ 2, that is, redshifts with a reliability $\gtrsim$ 80%.

2.3. Photometric data

We used photometric information from Suprime-Cam data for the MACS0329 field. Data were retrieved from CLASH page[3], available at the Mikulski Archive for Space Telescopes (MAST). A full description of the reduction of the Suprime-Cam images can be found in the data section of the CLASH website [4]. Briefly, the images were reduced by one of us using the techniques described in Nonino et al. (2009) and Medezinski et al. (2013). The total area covered by the images is 34×27 arcmin^2. Zeropoints are in the AB system. In particular, we retrieved the image in the R_C band with an exposure of 2400 s and a depth of 26.48 mag. The corresponding photometric catalog can be found on the website CLASH catalogs [5].

We also used data from the Panoramic Survey Telescope and Rapid Response System (Pan-STARRS, Flewelling et al. 2020). In particular, we extracted r, g, and i band magnitudes from the PS1-DR2 data release[6].

3. Selection of group members and catalog

Based on the measured spectra, the two BGGs are very close in velocity space at $z \sim 0.153$. The redshift distribution of the 1712 galaxies in the CLASH-VLT redshift catalog was analyzed using the 1D adaptive-kernel method of Pisani (1993, hereafter 1D-DEDICA). This distribution reveals a peak of galaxies at $z \sim 0.45$ corresponding to MACS0329, as well as several other foreground and background structures (Girardi et al. in prep.). Among these structures, the 1D-DEDICA method detects a foreground peak at $z = 0.153$. It consists of 59 galaxies, 32 of which are located in the southeastern region of MACS0329. We added these 59 galaxies from CLASH-VLT to the 18 galaxies from TNG. Our initial combined redshift catalog thus consists of 77 galaxies. Most of the TNG galaxies are brighter than $R_C = 20$ mag, while the data from CLASH-VLT include galaxies down to $R_C \sim 24$ mag.

To select group members among the 77 galaxies in our combined redshift catalog, we used the two-step method known as Peak+Gap (P+G, Girardi et al. 2015). The first step is to apply the 1D-DEDICA method with adaptive-kernel. With this, we detect a peak at $z \sim 0.1536$ with 41 galaxies in the range $45\,269 \leq V \leq 46\,858$ km s^{-1} (see Figs. 3 and 4). The nonmembers are 28 foreground and 8 background galaxies. In particular, there is a foreground peak at $z \sim 0.1435$, that is, at more than 2600 km s^{-1} in the foreground (cf. Sect. 6).

In a second step, we combine the space and velocity information in the "shifting gapper" procedure (Fadda et al. 1996; Girardi et al. 1996). Of the galaxies that lie within an annulus around the center of the system, this procedure excludes those that are too far away in velocity from the main body of galaxies (i.e., are farther away than a fixed velocity distance called the velocity gap). The position of the annulus is shifted with increasing distance from the center of the cluster. The procedure is repeated until the number of cluster members converges to a stable value. Fadda et al. (1996) suggested a velocity gap of 1000 km s^{-1} in the cluster rest-frame and an annulus size of 0.6 Mpc or more to include at least 15 galaxies. Since the two BGGs have comparable luminosities, we determine the center of the group by averaging their positions in right ascension (R.A.) and declination (Dec.) [R.A.=$03^h30^m06\overset{s}{.}73$, Dec.=$-02°18'24\overset{''}{.}8$ (J2000.0)].

[3] https://archive.stsci.edu/prepds/clash/
[4] https://archive.stsci.edu/missions/hlsp/clash/macs0329/data/subaru/
[5] https://archive.stsci.edu/missions/hlsp/clash/macs0329/catalogs/subaru/
[6] https://catalogs.mast.stsci.edu/panstarrs

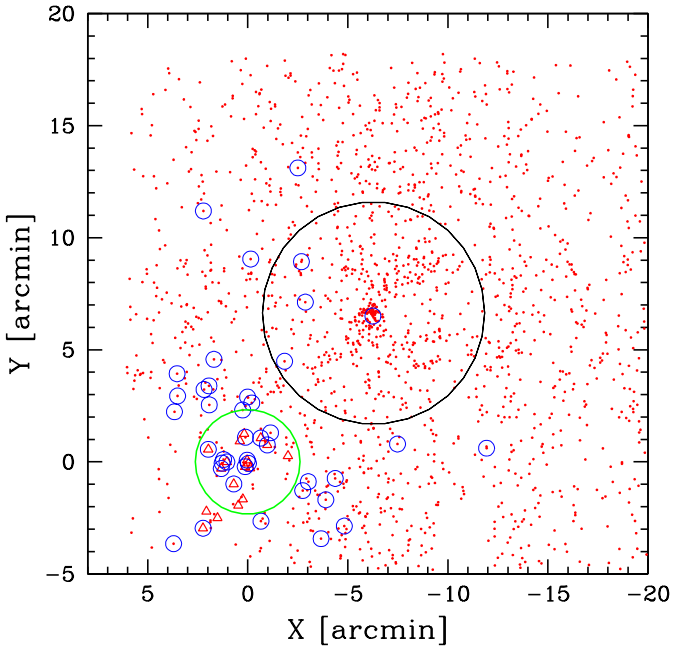

Fig. 3. Spatial distribution of all galaxies with redshift in the MACS0329 field. The large black circle indicates the R_{200} radius of the cluster. Red triangles and dots show galaxies with TNG and CLASH-VLT redshifts, 18 and 1712, respectively. The symbols outlined with blue circles indicate the 41 group member galaxies. The point 0,0 in the diagram indicates the center of GrG J0330-0218 and the green circle indicates the 0.5 R_{200} radius of the group (see also Fig. 1).

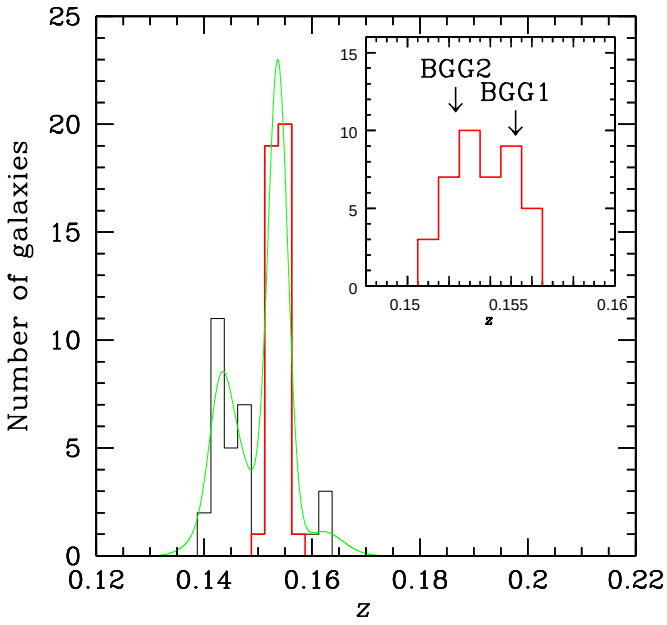

Fig. 4. Distribution of galaxies in our combined redshift catalog of 77 galaxies in the range $z = 0.12$–0.22. The histogram with the thick red line refers to the 41 galaxies that belong to the density peak of GrG J0330-0218, which was identified with the 1D-DEDICA reconstruction method (faint green line). The inset shows the 41 member galaxies with the redshifts of BGG1 and BGG2 indicated.

Following the procedure described above, the 41 group members are confirmed. Since a group is expected to have a small velocity dispersion, we also used the above procedure with a smaller velocity gap down to 500 km s^{-1}, always confirming the 41 group members. The position of the galaxies in the project phase-space is shown in Fig. 5. To highlight the region of the cluster members, we also plot the escape velocity curves, which were obtained using the recipe of den Hartog & Katgert (1996). We used the mass estimate calculated in the following section and assumed a Navarro-Frenk-White mass density profile (NFW, Navarro et al. 1997). Table 1, available in full at CDS, lists the velocity catalog for the member galaxies.

4. Group structure and properties

4.1. Global properties and galaxy population from optical data

Analysis of the velocity distribution of the 41 group members was performed using the biweight estimators for location and scale included in ROSTAT (statistical routines of Beers et al. 1990). Our measurement of the mean redshift of the group is $\langle z \rangle = 0.1537 \pm 0.0001$ (i.e., $\langle V \rangle = 46\,067 \pm 41$ km s^{-1}). We estimate the velocity dispersion, σ_V, by applying the cosmological correction and the standard correction for velocity errors (Danese et al. 1980). We obtain $\sigma_V = 369^{+20}_{-51}$ km s^{-1}, where the errors are estimated using a bootstrap technique.

We derive the mass M_{200} within R_{200}[7] using the theoretical relation between M_{200} and the velocity dispersion verified in simulated clusters (Eq. 1 of Munari et al. 2013). To obtain a first estimate of the radius R_{200} and the group mass M_{200} contained therein, we applied the relation of Munari et al. (2013) to the global value of σ_V which we obtained above. We considered the galaxies within this first estimate of R_{200} to calculate a new value for the velocity dispersion. The procedure is repeated until we obtain a stable result that estimates $\sigma_{V,200} = 389^{+23}_{-71}$ km s^{-1} for 28 galaxies within $R_{200} = 0.77^{+0.05}_{-0.14}$ Mpc. We derive $M_{200} = 6.0^{+1.7}_{-3.9} \times 10^{13}\ M_\odot$. The uncertainties for R_{200} and M_{200} are calculated using the error propagation of $\sigma_{V,200}$ ($R_{200} \propto \sigma_{V,200}$ and

[7] We denote R_Δ as the radius of a sphere within which the average mass density is Δ times the critical density at the redshift of the galaxy system; M_Δ is the mass contained in R_Δ.

Table 1. Radial velocities of 41 member galaxies of GrG J0330-0218

ID	R.A., Dec. (J2000) [h : m : s, ° : ′ : ″]	r [mag]	V [km s^{-1}]	ΔV	Source
01	03 30 06.85 − 02 18 20.3	16.68	46528	153	T
02	03 30 06.60 − 02 18 28.9	17.01	45666	93	T
03	03 30 07.76 − 02 16 06.0	17.15	46858	75	V
04	03 30 21.57 − 02 22 03.9	17.36	45988	150	V
05	03 30 12.02 − 02 18 42.7	18.20	45349	84	T

Notes. Full table is available at CDS. We list: identification number of each galaxy, ID; right ascension and declination, R.A. and Dec. (J2000); r-band magnitude; heliocentric radial velocity, $V = cz$, with error, ΔV; source of spectroscopic data (T: TNG, V: VIMOS-VLT, M: MUSE-VLT). IDs. 01, 02, and 03 are BGG1, BGG2, and BGG3, respectively. Magnitudes are generally Pan-STARRS Kron-like r magnitudes from PS1 mean data. Those with note 'a' are obtained from PS1 stacked data and those with 'b' are obtained from Suprime R_C catalog and converted ($r = R_C + 0.25$, Fukugita et al. 1995).

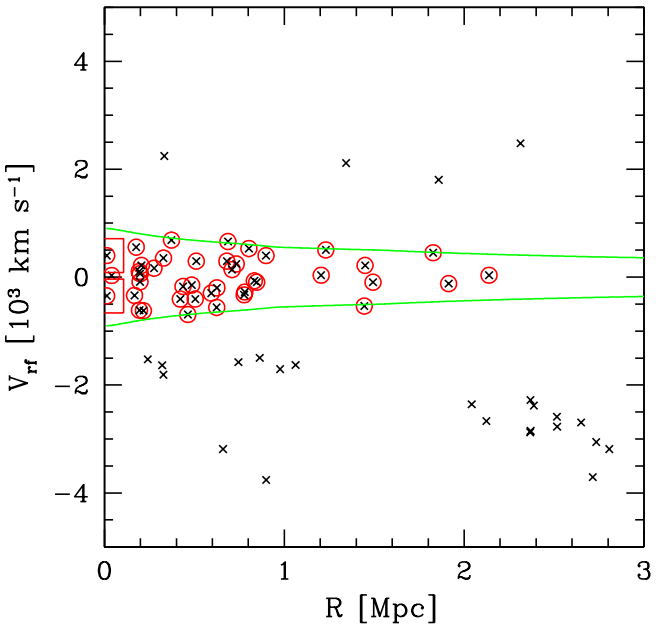

Fig. 5. Rest-frame velocity $V_{\rm rf} = (V - \langle V \rangle)/(1+z)$ vs. projected group-centric distance R for galaxies with redshifts in the range ± 5000 km s^{-1} (black crosses). The red circles show the 41 members of GrG J0330-0218. The large red squares refer to BGG1 and BGG2. The green curves contain the region where $|V_{\rm rf}|$ is smaller than the escape velocity (see text).

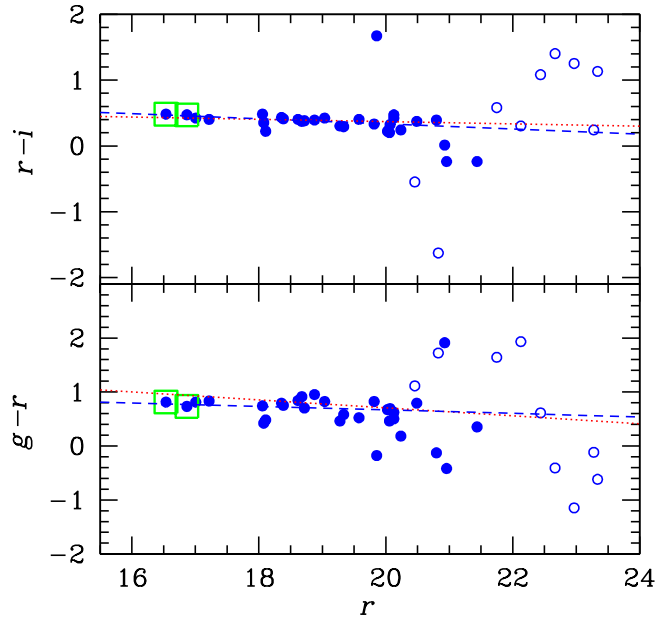

Fig. 6. Pan-STARRS aperture-color vs. Kron-like magnitude diagrams $r - i$ vs. r and $g - r$ vs. r in lower and upper panels, respectively). All member galaxies are shown with the exception of two very faint galaxies for which PS1 magnitudes are not available. The full circles indicate data obtained from PS1 mean data and open circles those available only as stacked data. The large green squares indicate BGG1 and BGG2. The blue dashed lines show the color-magnitude relations obtained for the member galaxies. The red dotted lines show the relations taken from the literature (see Sect. 7).

$M_{200} \propto \sigma^3_{\rm V,200}$) and an additional uncertainty of 10% for the mass due to the scatter in the relation of Munari et al. (2013). The properties of the group are shown in Table 2.

Using a number of indicators such as kurtosis, skewness, tail index, and asymmetry index (Bird & Beers 1993), the analysis of the velocity distribution shows no evidence of possible deviations from the Gaussian distribution. We find no evidence of substructure in the 3D distribution (velocity+positions) using the classical Δ-test of Dressler & Shectman (1988) or slightly modified versions (Girardi et al. 2010).

BGG1 has a higher velocity than the mean cluster velocity, as shown in Fig. 4 (inset). According to the Indicator test (Gebhardt & Beers 1991), the velocity of BGG1 is peculiar at the > 99% c.l.. However, if we consider the two dominant galaxies BGG1 and BGG2 together, that is, their average velocity and not only the velocity of BGG1, we do not find any peculiarity.

We have also analyzed the position of the group galaxies in the color-magnitude diagrams. We can assign Pann-STARRS magnitudes to all member galaxies, except for two very faint galaxies with $R_{\rm C} > 23$ mag. Figure 6 shows the distribution of member galaxies in the color-magnitude diagrams $r - i$ vs. r and $g - r$ vs. r. In Fig. 6 the magnitudes are corrected for Galactic foreground extinction (Schlafly & Finkbeiner 2011). The color-magnitude relations can be seen down to faint magnitudes $r \sim 20$ mag. We use the galaxies with $r < 20$ and the 2σ rejection procedure of Boschin et al. (2012) to fit $r - i = 1.115 - 0.039 \times r$ and $g - r = 1.308 - 0.032 \times r$.

Then we calculated the total luminosity of the galaxies $L_{\rm gals}$ within $0.5\,R_{200}$. There, the redshift completeness is about ∼ 75% at the magnitude limit of $19.68 = r_{\rm BGG1} + 3$. Of the 21 Pan-STARRS galaxies brighter than the magnitude limit, we have the redshift for 16 galaxies: nine and seven galaxies are members and nonmembers, respectively. Of the five galaxies with no spectroscopic redshift, the giant spiral galaxy with a diameter ∼ 0.′8 at the eastern $0.5\,R_{200}$ limit is likely a foreground galaxy (labeled with "Spi" in Fig. 1). We classify it as a nonmember galaxy. This assumption is also confirmed by our estimate of the photometric redshift $z_{phot} = 0.11 \pm 0.02$ obtained with the algorithm of Tarrío & Zarattini (2020). We thus define two samples of galaxies: one consisting of the nine spectroscopic members and one consisting of the nine members plus the four galaxies without redshift. We corrected magnitudes for extinction, the K-correction, and the evolution correction (Eq. 2 in Girardi et al. 2014), and summed the luminosities of all galaxies to obtain a range of values for the global galaxy luminosity within the magnitude limit, $L_{\rm obs}$. The contribution from the fainter galaxies is estimated using the Schechter luminosity function according to the procedure in Girardi et al. (2014). We obtain $L_{\rm gals} = L_{\rm obs} + L_{\rm faint} = 4.0 \times 10^{11}\ L_\odot$ and $4.6 \times 10^{11}\ L_\odot$ for the two samples of 9 and 13 galaxies, respectively. A 17% of luminosity is due to the magnitude corrections and a 19–25% is due to the extrapolation to faint galaxies. We used the NFW profile to calculate the projected mass within $0.5\,R_{200}$ and obtained a mass-to-light ratio $M/L \sim 130\ M_\odot/L_\odot$.

4.2. Analysis of X-ray data

GrG J0330-0218 was serendipitously observed by *Chandra* with the Advanced CCD Imaging Spectrometer (ACIS, Garmire et al. 2003) within the field of view of four observations of MACS J0329.6-0211 (Observations ID: 7719, 3257, 3582, 6108). The data set was reprocessed and cleaned following the steps described in Bartalucci et al. (2017, see their Appendix A). We briefly report the procedures here. Data were processed using

Table 2. Global properties of GrG J0330-0218

N_{gal}	R.A, Dec. J(2000) [h : m : s, ° : ′ : ″]	< z >	σ_V [km s^{-1}]	$\sigma_{V,200}$ [km s^{-1}]	R_{200} [Mpc]	M_{200} [$10^{13} M_\odot$]
41	03 30 06.73, −02 18 24.8	0.1537 ± 0.0001	369^{+20}_{-51}	389^{+23}_{-71}	$0.77^{+0.05}_{-0.11}$	$6.0^{+1.7}_{-3.9}$

Chandra Interactive Analysis of Observations (CIAO, Fruscione et al. 2006) version 4.13 using the latest calibration files updated to version 4.9.6. High-energy particle contamination was reduced by using the Very Faint mode[8]. Observational periods affected by flares were removed following the procedures of Hickox & Markevitch (2006) and Markevitch (2006). The four observations were merged after the cleaning procedure to maximize the statistics. The resulting total cleaned exposure time is 55 ks. The exposure-corrected image in the 0.5–2.5 keV band was obtained by combining the four observations.

GrG J0330-0218 is in the outermost part of the field of view. The distance to the aim-point is on average 10′, and for this reason any diffuse emission of the group is expected to be weak. At the position of GrG J0330-0218, the only emission visible on the image is point-source like and centered on BGG1. We investigated the nature of this emission by comparing the surface brightness profile extracted from the group with that of a point source at the same distance from the aim-point. The profile of the group was extracted from concentric annuli centered on the BGG1 position, thus considering both BGG1 and possible intragroup medium. We computed the background-subtracted and exposure-corrected average surface brightness profiles in each annulus. The technique of extraction is detailed in Bartalucci et al. (2017). The direct comparison of the background-subtracted and exposure-corrected surface brightness profiles is shown in Fig.7. We scaled the surface brightness profiles intensity by their maximum value and we applied an offset of to the radial grids so that the first bins of the profiles coincide. The group emission is systematically above the point source at $R > 0.'2$, $\sim 12''$, and the point source profile decreases rapidly. The 90% average encircled energy fraction at 1.49 keV is within $\sim$ 10 arcsec[9], which is consistent with the point source profile. The group emission extends to 1′, indicating the presence of a faint extended emission. In addition, the surface brightness profiles are binned to have at least 3σ in each bin. That is, we have found that the surface brightness profile extracted from the group is consistent with extended emission. The extended emission is centered exactly on the galaxy BGG1. We cannot tell whether the observed extended emission is originated from the diffuse hot gas embedded in the halo of the group or rather from BGG1 itself. A dedicate observation is needed to separate the two components and determine the key thermodynamic quantities.

5. Bright group galaxies and diffuse light

Inspection of the Suprime-Cam R_C image reveals a clear signature of diffuse light around the two central galaxies (see Fig. 1). In particular, one can see a distinct tail in the southeastern part of BGG2. In Sect. 5.1, we first focus on the photometric decomposition of the surface brightness profiles of the two BGGs to understand the morphological type of these galaxies. Then, in Sect. 5.2 the ICL is calculated using the surface brightness cut technique (hereafter SB cut).

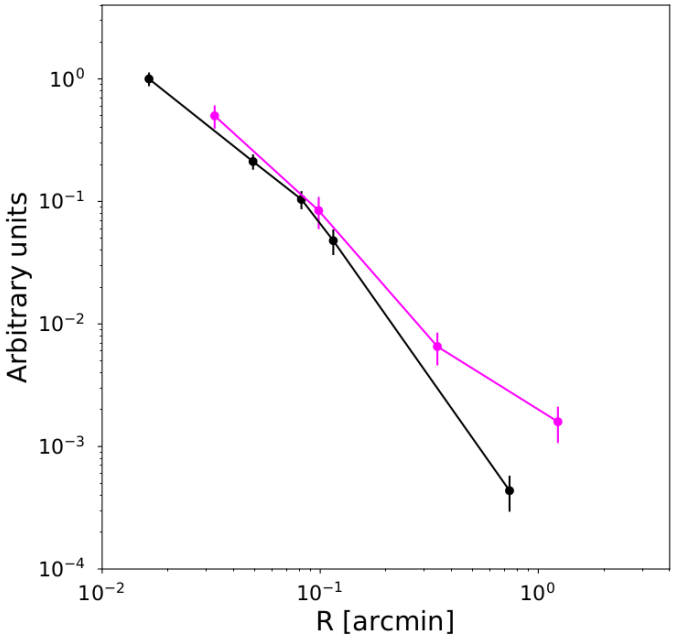

Fig. 7. Surface brightness profiles of the two X-ray sources. The group and point sources are shown by magenta and black lines. Both profiles are extracted in the 0.7–2.5 keV band.

5.1. Photometric decomposition of the two dominant galaxies

The photometric decompositions were performed using the GASP2D code (Méndez-Abreu et al. 2008, 2014, 2017). The method is able to fit several components to the surface brightness profile of the galaxy. In particular, the latest version of GASP2D is able to account for a bulge, a disk with no or negative or positive bending, up to two bars, and a nuclear source to mimic the AGN in the central region. Details of the method and its configuration can also be found in de Lorenzo-Cáceres et al. (2020). The PSF is taken into account in the decomposition. In particular, we measure the FWHM of a set of nonsaturated stars in the image (identified using SDSS data) with a Moffat function. The resulting mean PSF is used in GASP2D as a kernel to be convoluted with the model of each galaxy, thus the final model is seeing-corrected (Méndez-Abreu et al. 2017). The sky level was evaluated using the IRAF task `imexam`: we measured 10 different (empty) regions of the sky, getting for each region the mean value over an area of 25 pixels. We then computed the average value of the sky from these 10 measurements. In Figs. 8 and 9 we show the results of the photometric decomposition of BGG1 and BGG2, respectively.

The most interesting result of the decomposition is that BGG1 clearly has a disk component. Disks are fragile structures,

[8] https://cxc.harvard.edu/cal/Acis/Cal_prods/vfbkgrnd
[9] Fig. 4.12 of the *Chandra* proposal observatory guide cxc.harvard.edu/proposer/POG/html/chap4.html